Structural Safety 102 (2023) 102285



Contents lists available at ScienceDirect

Structural Safety

journal homepage: www.elsevier.com/locate/strusafe





On the existing test dataset of isotropic cylindrical metal shells under axial compression and the design of modern metal civil engineering shells

Adam J. Sadowski [a], Maria Terres Morata [a], Lijithan Kathirkamanathan [a], Marc Seidel [b], J. Michael Rotter [a,c]

[a] Department of Civil and Environmental Engineering, Imperial College London, UK
[b] Siemens Gamesa Renewable Energy GmbH & Co KG, Germany
[c] The University of Edinburgh, UK

ARTICLE INFO

Keywords:
Shell buckling
Metal civil engineering shells
Uniform axial compression
Imperfections
Out-of-roundness
Load application non-uniformity
Non-parametric hypothesis testing
Bootstrapping
Monte Carlo simulation

ABSTRACT

In the structural engineering limit state design philosophy of the Eurocodes, a target reliability is achieved by using partial safety factors on both the loading and the resistance that are, in principle, to be calibrated based on test data. The partial factor that is currently used for the buckling limit state of metal shells has been adopted from the knowledge base on other structural elements and has been retained for reasons of historical continuity and to maintain a close relationship between all Eurocode steel design standards. However, the mechanics of the behaviour of thin-walled metal shells gives strong reasons to believe that the partial factors for buckling should be dependent on the shell geometrical form, slenderness, load case and quality of fabrication for the target reliability to be consistently achieved. None of these are currently considered in defining the partial factor for resistance.

The most ubiquitous thin-walled metal shell structures are imperfection-sensitive cylinders under uniform axial compression. A dataset of many hundreds of these test results has thus been accumulated over many decades, though it is of variable quality and sparsely documented. This paper shows that this dataset is an entirely inappropriate basis on which to calibrate the safety level of full-scale metal civil engineering shells. Indeed, the professional community should face the uncomfortable reckoning that an experimental test dataset suitable for the reliable calibration of the safety level of design relationships for full-scale metal civil engineering shells may likely never come into existance, and that the bolder approach of extensive computational simulation must instead be embraced.

1. Introduction

It has been known for over a century that the buckling strengths of thin isotropic cylindrical shells under uniform axial compression fall significantly below the classical theoretical predictions of Lorenz [1] and Timoshenko [2] which are based on small-deflection elastic treatments assuming a perfect shell geometry. The discrepancy between theory and experiment was eventually identified by Koiter [3] as being caused by the severely unstable post-buckling response and consequent sensitivity to geometric imperfections which are inevitably present in test specimens (see the extensive historical accounts in Singer *et al.* [4] and Elishakoff [5–8]). The prediction of realistic buckling strengths of imperfect shells required the development of nonlinear shell theories [9–13], coupled with an improved quality and quantity of information on imperfections present in the tested specimens (e.g. the GALCIT system at Caltech, and [4,14–16]) and increasingly powerful computers on which sophisticated computational models could trace complex nonlinearities and process data (see historical account in Bushnell [17]), all of which developed relatively slowly over several decades. Consequently, for a long time the design of cylindrical shells under any load case proceeded on the basis of simple algebraic formulae representing empirical lower-bound estimates of resistances derived from tests. Given the economic importance of the axially compressed cylinder to industrial applications, the relative ease of testing shells under these conditions and its status as the chief reference case for more complex load conditions, it has historically been the most tested shell system producing the largest test dataset [4,18].

2. Destructive testing, imperfection surveying and design of shells

Numerous attempts at compiling datasets of test results of isotropic axially compressed cylinders have also tried to validate the several existing design resistance equations by using lower bounds on the tests.

https://doi.org/10.1016/j.strusafe.2022.102285
Received 26 November 2021; Received in revised form 13 September 2022; Accepted 15 September 2022
Available online 24 February 2023
0167-4730/© 2022 The Author(s). Published by Elsevier Ltd. This is an open access article under the CC BY license (http://creativecommons.org/licenses/by/4.0/).

These include those of Harris *et al.* [19] (from 1957; approximately $n \approx 190$ specimens), Weingarten *et al.* [20] (from 1965, Fig. 3 therein; $n \approx 300$ specimens), Schulz [21] (from 1981; $n \approx 210$ specimens) as reported by Ummenhofer [22] and Waeteraere [23] (from 1988; $n > 750$ specimens) as reported by Schmidt [24]. Most recently, a dataset of 517 buckling test results was compiled by Wagner *et al.* [25], partly from the same legacy data as the above datasets and partly from more recent tests performed by Jiao *et al.* [26] and Wang *et al.* [27–28]. In the aerospace sector, it is the dataset of Weingarten *et al.* [20] that appears to have been the most influential, forming the basis of the empirical buckling rules of the NASA SP-8007 [29] guidelines from 1965 that continue to be used in launch vehicle design to this day. More is said on civil engineering shells shortly.

Following the discoveries of Koiter [3,30], the importance of quantifying both the form and amplitude of specimen geometrical imperfections was recognised (e.g. [31–32]) and detailed surface imperfection surveys began to be undertaken for aerospace research (e.g. [14–15]). In fact, Singer *et al.* [4] (see p. 820 therein) indicated that prior to the 1970s such measurements would have been considered 'useless and bothersome' by most experimenters who would also have had difficulty in making them. The zenith of aerospace imperfection surveying was the (now entirely defunct) Initial Imperfection Data Bank once hosted at TU Delft [4,33] which stored full 2D Fourier decompositions of surface imperfection surveys of shells for aerospace research that allowed the imperfect geometry to be reproduced with good fidelity. The experiments at INSA de Lyon (e.g. [34]) then took this process much further by laser tracing the changing complete shape of each specimen throughout the loading process, sometimes seeing the transformation of smaller imperfections into failure whilst more prominent imperfections in the unloaded shell had less effect. A large newly constructed civil engineering shell [35] was also treated to Fourier decomposition by Teng *et al.* [36], and modern experimentalists can now achieve very high-resolution surface imperfection surveys of cylindrical specimens using laser instrumentation e.g. [27–28,34,37–42]. In theory, these can be processed into nodal coordinates for direct analysis with a nonlinear finite element program to closely reproduce the experimentally-obtained buckling resistances. But despite these modern technical advances, most of the legacy tests for metal shells under axial compression that form the current datasets do *not* contain appropriate quantitative information on the quality of the specimens. Of those that do, the information reported even in relatively recent publications (e.g. [43]) is often insufficient to recreate the key features of the imperfect shell geometry comprising both long-wave (e.g. out-of-roundness or ovalisation) and short-wave (e.g. dimples and wavelengths, weld joints) imperfections.

Research on the design of aerospace vehicles under axial compression has historically sought to find a lower-bound to possible (predominantly elastic) strengths, defined as a 'knockdown factor' on the reference classical elastic critical buckling stress to account for the destabilising effect of surveyed or postulated geometric imperfections as a function of the radius to thickness (r/t) ratio or another dimensionless slenderness group. Several authors acknowledge that much of the test dataset is old and that knockdown factors derived from it are no longer fit for purpose e.g. [28,33]. For aerospace applications, some attempts are in progress to reduce the conservatism of the empirical NASA SP-8007 [29] rule by updating the database and expanding it to include composite materials and stiffened construction. New test programmes, using more carefully constructed and loaded specimens that exhibit higher resistances (e.g. [27,44]) and sophisticated computational, and often probabilistic, treatments are gradually supplementing the test dataset (e.g. [5,28,39,45–47]).

In civil engineering, the development of the 1980, 1984 and 1988 versions of the European Design Recommendations on the Buckling of Shells used the dataset of Schmidt and Waeteraere (hereafter termed the 'German dataset') that had been compiled for the German steel shell buckling standard DIN 18800-4 [48] in 1990. However, it is quite unjustifiable to assume that it would always be safe to draw a lower bound drawn on a widely varying set of model tests in laboratories with unknown imperfections of both geometry and loading. Even if such a lower bound could somehow be justified on the grounds that no shells could be weaker than these test results, this bound still fails to give any indication of the tolerances required to meet this lower bound and the quality of fabrication needed for its use in full-scale structures. As described by Rotter [49–50], different authors have proposed different strategies to define the safe resistance of shells, but the only one that leads to safe design coupled with defined tolerances for use in construction is the identification of the likely worst possible imperfection form for a given loading, coupled with accurate prediction of the reliable resistance for a given imperfection amplitude. This was adopted into the first draft of the European Eurocode on shell buckling ENV 1993-1-6 [51] in 1999 following the proposal of Rotter [52–53] and allows three different Fabrication Tolerance Quality Classes to be chosen by the designer and implemented by tolerance measurements into construction. The predictions were slightly updated for the formal publication of EN 1993-1-6 [54] in 2007 and compared to the German dataset by Schmidt *et al.* [55]. The German dataset has also been exploited as the experimental data in a partial factor calibration exercise by Sørensen and Toft [56] and used in the development of the IEC 61400-1 [57] international standard on wind turbines from 2019. There is a significant overlap between the Weingarten and German datasets.

The Eurocode EN 1993-1-6 [54,58] is a state-of-the-art document that follows the reliability framework of partial factors on loading and resistance set out in EN 1990 [59]. Using the notation of Rotter [60], a characteristic resistance R_k is established based on testing or theory that 95% of structures of a particular class and failure mode will meet or exceed. It is then transformed into a design resistance R_d to be met or exceeded by 99.9% of them through a partial factor γ_M such that $R_d = R_k / \gamma_M$. For the buckling limit state, and regardless of shell geometry, slenderness or load condition, the ENV 1993-1-6 [51] in 1999 and EN 1993-1-6 [54] in 2007 on metal shells adopted the partial factor $\gamma_{M1} = 1.1$ to be compatible with the buckling factor used for structural members in EN 1993-1-1 [61] without rational justification. The earlier German standard DIN 18800-4 [48] for shells had used this value only for thick shells, with a higher value for 'very' imperfection-sensitive shells (such as cylinders under uniform axial compression and spheres under uniform external pressure) so that γ_M varied from 1.1 for thicker shells to 1.45 for very thin ones. The increased safety level at higher slendernesses was deemed necessary because of the significant experimental scatter seen in tests on slender shells (illustrated shortly) and their increasingly unstable post-buckling behaviour. Unfortunately, this progressive distinction was not adopted into EN 1993-1-6 [54,58].

For thick-walled cylindrical geometries, detailed reliability studies and partial factor calibrations have been carried out for circular hollow sections (CHS) to provide rules for the Eurocodes EN 1993-1-1 [61] and EN 1993-1-4 [62] on carbon and stainless steel structural members respectively [63–68]. The partial factors were found using an extensive dataset of hundreds of tests and based on the first order reliability method (FORM) presented in EN 1990 Annex D [59]. These tested thicker laboratory specimens do certainly closely represent structural members used in building construction. They are manufactured to carefully controlled tolerances, rather than fabricated on site, leading to specimens of high quality, with imperfections and residual stresses that are representative of those in construction. The plasticity-dominated limit state resistances of these CHS thick shells are also quite insensitive to imperfections, in strong contrast to the severe imperfection sensitivity of thin shells.

3. Aims and scope of the present study

This study first aims to compile and explore a detailed dataset of test results for cylindrical isotropic thin metal shells under uniform axial compression that broadly reconstitutes the influential German dataset that is now understood to be irrecoverably lost (Prof. Herbert Schmidt,

personal communication). To this end, a dataset of 648 test results sourced from the publicly available literature was processed and categorised according to how the specimens were likely to have been fabricated to permit a systematic computational treatment of different widely used types of specimens. Six broad specimen fabrication categories were identified, with a seventh 'miscellaneous' category reserved for specimens where the manner of fabrication either could not be discerned unambiguously e.g. [69] or would have formed a very small cluster (e.g. the spiral-welded specimens of Dongxu *et al.* [70]). Non-parametric hypothesis testing was then used to explore to what extent this collected dataset is statistically similar to the German dataset to establish whether it can be treated as its ersatz for further study.

Once the ersatz is established, the reconstruction will provide empirical probability distributions of basic geometric and material variables of the largest subgroup within the dataset, found to be for specimens fabricated by overlapped longitudinal joining, for subsequent Monte Carlo sampling. These longitudinally overlapped-joined specimens were found to have among the lowest experimentally obtained buckling resistances and to cover a wide range of dimensionless slenderness relevant to different civil engineering metal shell applications. The selection of these specimens permitted the postulation of an idealised algebraic representation of systematic geometric imperfections related to this fabricated geometrical form. Using a combination of nonlinear finite element analysis, Monte Carlo simulation and bootstrapped hypothesis testing, it will be shown here that the geometric and loading imperfections that may have existed in this subset of laboratory specimens are unlikely to represent construction methods used in large-scale civil engineering metal shells. The paper ends by presenting the Authors' vision of the future direction that research into thin metal shell structures should adopt if it is to remain both meaningful to design practice and a state-of-the-art research field.

During the review of this manuscript the Authors were advised that a study analogous to the first part of the present work was conducted by B. P. Makarov in the Soviet Union in the early 1960s [71–73]. These references are provided here for completeness.

4. Reconstruction of the test dataset

As noted above, a detailed data collection exercise was carried out to compile a large and well-documented dataset of buckling tests on unstiffened isotropic cylinders under axial compression prior to subsequent Monte Carlo analysis. References were sourced from articles, research reports, dissertations and books, with the 1120-page volume of Singer *et al.* [4] proving to be a particularly valuable resource. Only metallic shells were included, though this eliminated many tests on mylar polymer shells that influenced the NASA SP-8007 [29] rules [13,20,74]. The full list of sources is too long to be reproduced here but may be found in the supplementary materials for this article. The Authors acknowledge that this dataset is not exhaustive, but it is sufficiently representative to permit widely relevant and valuable conclusions to be drawn.

4.1. Graphical summary

The collected dataset is summarised graphically in Fig. 1 in terms of different versions of a capacity relationship between a dimensionless buckling resistance against a dimensionless slenderness. The first plot, Fig. 1a, shows χ against λ where:

$$\chi = \frac{R_k}{R_{pl}} \text{ and } \lambda = \sqrt{\frac{R_{pl}}{R_{cl}}} \text{ with}$$
$$R_{pl} = f_y A = 2\pi f_y rt \text{ and } R_{cl} = f_{cl} A = \frac{2\pi Et^2}{\sqrt{3(1-\nu^2)}} \tag{1}$$

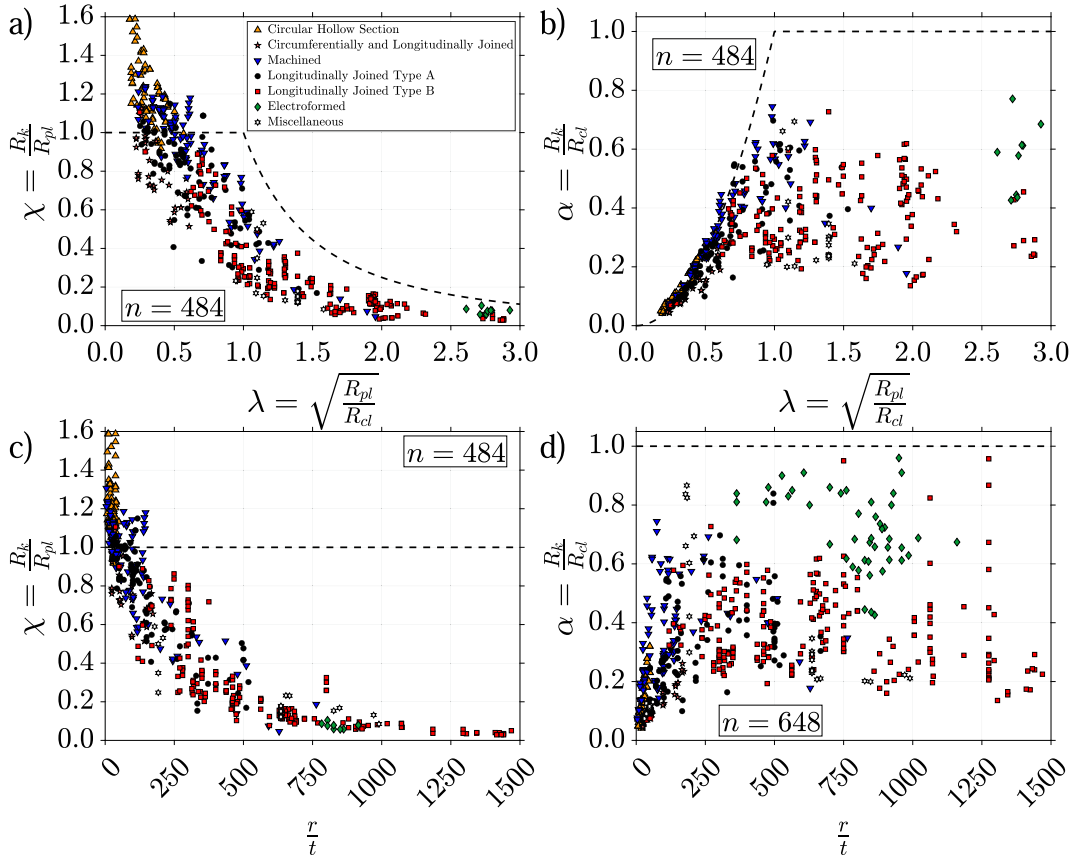


Fig. 1. Graphical summary of up to 648 tested cylinders under axial compression grouped according to specimen fabrication category and plotted as dimensionless buckling resistances χ or α against dimensionless slenderness λ or r/t.

such that R_k is the 'characteristic' resistance of the tested specimen under the nominal load case of uniform axial compression, while R_{pl} and R_{cl} respectively are the reference plastic and elastic critical buckling resistances of the perfect cylindrical shell as identified by a radius r and thickness t, yield stress f_y, elastic modulus E and Poisson's ratio ν. This follows the framework and notation of Rotter [60] and EN 1993-1-6 [54,58]. Measured geometric and material properties were used in preference to nominal ones wherever both were reported. Previous sources to have compiled a similar image include Schmidt [24,55,75], to which the present image bears a strong similarity. Fig. 1b) presents an alternative view in terms of a dimensionless resistance relative to the elastic critical buckling value expressed as:

$$\alpha = \frac{R_k}{R_{cl}} \tag{2}$$

For completeness, Fig. 1c) and d) respectively display the dataset as χ and α against r/t, with d) in particular being directly comparable with similar figures produced by Weingarten *et al.* [20] or Wagner [25] where α is referred to as the 'knockdown factor' on the reference elastic critical buckling resistance R_{cl}.

A presentation of the data with the dimensionless length taken either as the Batdorf parameter $Z = L^2/(rt\sqrt{(1-\nu^2)})$ or as $\Omega = (L/r)\sqrt{(t/r)}$ to make it invariant with the cylinder length is also possible e.g. [44]. However, most of the cylinders identified in this dataset are classified as being of 'medium' length ($\Omega < 2.86$) where the buckling resistance under axial compression is chiefly independent of length [58,76]. It should be added that λ is a much more general slenderness metric than the r/t ratio since it permits scale invariance with the material properties f_y and E in addition to the geometry. The image in Fig. 1d) may perhaps surprise some readers who would expect the 'cloud' of data to converge towards $\alpha = 1$ as $r/t \to 0$, as may be seen in Weingarten *et al.* [20] and others, rather than towards $\alpha = 0$ as is seen here. This arises because much of the previously presented data covered only elastic cylinders (chiefly mylar), whilst the present dataset includes thicker cylinders that fail plastically at low r/t, and since $R_k \approx R_{pl}$ for such cylinders it may be shown algebraically using Eq. (1) that $R_k / R_{cl} \approx R_{pl} / R_{cl} \to 0$ as $r/t \to 0$. Previous graphical displays of cylinder test strengths under axial compression are likely to have been limited to specimens that buckled predominantly elastically even when relatively thick-walled, giving the appearance of a tendency towards $\alpha = 1$ as $r/t \to 0$. Moreover, as noted above, α was historically defined only as a knockdown factor on the elastic buckling condition R_{cl}, with plastic buckling not having been the focus of most research endeavours. It is also of interest to note that for $r/t > \sim 250$, $\alpha \approx 0.2$ seems to provide a consistent lower bound to the elastic buckling resistances.

The graphical summary in Fig. 1 tells a familiar story: the combined dataset exhibits a significant scatter across all slendernesses and most high-slenderness cylinders fail significantly below the classical theoretical prediction of R_{cl}. For stocky cylinders (low λ or r/t) which are predominantly either steel or aluminium CHS tubes and machined and thick welded cylinders, the plastic reference resistance R_{pl} is routinely exceeded due to post-yield strain hardening. The large scatter observed for these specimens is partly a consequence of the intrinsic variability exhibited by the post-yield strain hardening properties of metals (see the study of Sadowski *et al.* [77] on carbon steels) and partly as a result of the varying manner in which the yield condition may have been reported by the different experimenters to calculate R_{pl} (e.g. 0.2% proof stress, nominal stress, yield plateau stress etc.).

Thicker specimens fail by elastic–plastic buckling, but high slenderness specimens fail entirely by elastic buckling as R_{cl} takes over from R_{pl} as the reference condition (it may be noted that R_{cl} should be a strict upper bound that should not be able to be exceeded unless the specimen is exceptionally short [13,76]). The reason why some very slender cylinders (high λ or r/t) show both a large scatter and some very low buckling resistances relative to R_{cl} has usually been attributed to different kinds of imperfections in the tested assembly. Sensitivity to geometric imperfections is invariant with slenderness if the form and amplitude are kept constant relative to the wall thickness (see Fig. 2 in Rotter [78] or Fig. 14 in Fajuyitan and Sadowski [79]). However, it is very difficult to build thin model cylinders to tight tolerances, so both systematic and random imperfections are usually deeper, typically leading to lower buckling resistances. There is also evidence that non-uniformities in the load introduction may cause local compressive stress peaks in the shell that trigger early buckling [39,44] and that this effect may increase with slenderness [22], a phenomenon that will be illustrated later in this study. Unfortunately, the geometric and loading imperfections that may have existed in the tested shells, crucial to a correct interpretation of this data, are now forever unknowable. Additionally, as many references did not report the yield stress of the material at all, only 484 of the 648 shown in Fig. 1d) are shown in the remaining plots.

4.2. Statistical summary

The 484 specimens for which a yield stress was available and thus could be expressed on a χ vs λ relationship were grouped into narrow slenderness bands. Those that fell within the range $(\lambda_i - 0.125) < \lambda_i < (\lambda_i + 0.125)$ were classed into a single 'λ-bin' associated with a single value of λ_i at multiples of 0.25. These λ-bins were used to compute boxes-and-whiskers (Fig. 2a) and other summary statistics (listed in Table 1 to two significant figures purely for presentation purposes; the precision of these measurements is unknowable). The boxes denote the range between first and third quartiles of the resistances χ within a given λ-bin, a median line and mean dot are also shown, while whiskers denote the extremities of the resistances (excluding any data considered as outliers: that is, those exceeding 1.5 times the interquartile range beyond the first or third quartile). Consistent with Fig. 1, the dispersion relative to the mean value of every λ-bin is seen to be high, as assessed by the coefficient of variation (CV), which increases slightly with slenderness.

Table 1
Descriptive statistics of the specimen resistance χ grouped by λ-bin.

$\lambda_i \pm 0.125$ bin	# Entries	Min.	Max.	Median	Mean	Standard deviation	CV (%)	Skew	Excess kurtosis
0.25	103	0.70	1.8	1.1	1.1	0.22	19	0.33	0.0091
0.50	122	0.41	1.3	0.98	0.95	0.19	20	−0.61	−0.32
0.75	54	0.33	1.1	0.73	0.71	0.18	25	−0.36	−0.00023
1.00	68	0.17	0.78	0.42	0.42	0.15	37	0.35	−0.77
1.25	36	0.13	0.53	0.26	0.27	0.095	35	0.72	0.087
1.50	25	0.085	0.38	0.16	0.18	0.064	36	1.1	1.7
1.75	19	0.058	0.21	0.087	0.11	0.048	45	1.0	−0.36
2.00	36	0.035	0.16	0.11	0.11	0.038	36	−0.54	−0.74
2.25	4	0.060	0.11	0.078	0.082	0.024	30	0.33	−1.5
2.50	1	0.086	0.086	0.086	0.086	n/a	n/a	n/a	n/a
2.75	13	0.029	0.10	0.058	0.058	0.022	38	0.39	−0.46
3.00	3	0.029	0.080	0.035	0.048	0.028	58	0.67	−1.5

Table 2
Non-parametric normality and equality of distribution test p values grouped by λ-bin (small-sample p values should be treated with care).

$\lambda_i \pm 0.125$ bin	Normality tests (H_0: sample is normally distributed)			Equality of distribution tests (H_0: samples come from the same population)			Sample sizes	
	Anderson-Darling test	Lilliefors test	Shapiro-Wilk / Francia test	Kolmogorov-Smirnov test	Mann-Whitney-Wilcoxon test	Kruskal-Wallis test	Present work	German dataset*
0.25	0.38	0.44	0.30	0.00067	0.00099	0.00067	103	99
0.50	**0.00072†**	**0.017**	**0.00057**	0.015	0.016	0.015	122	75
0.75	0.075	0.069	0.11	**0.41‡**	**0.58**	**0.41**	54	35
1.00	**0.012**	0.051	**0.012**	**0.59**	**0.80**	**0.58**	68	40
1.25	0.21	n/a	0.12	**0.82**	**0.93**	**0.81**	36	24
1.50	0.089	0.17	**0.021**	**0.087**	**0.064**	**0.08**	25	18
1.75	**0.00066**	**0.010**	**0.0021**	**0.21**	**0.39**	**0.20**	19	23
2.00	**0.0077**	**0.0043**	**0.011**	0.031	0.015	0.030	36	30
2.25	0.59	n/a	0.54	**0.20**	**0.29**	**0.19**	4	16
2.50	n/a	n/a	n/a	n/a	n/a	n/a	1	6
2.75	0.25	0.27	0.30	n/a	n/a	n/a	13	n/a
3.00	n/a	n/a	n/a	n/a	n/a	n/a	3	n/a

† p values less than 0.05 indicate that samples from the present dataset in the given λ-bin are unlikely to be normally distributed at the 5% significance level (reject H_0);
‡ p values greater than 0.05 indicate that samples from the present test dataset and those from the German dataset in the given λ-bin are likely to have originated from the same population at the 5% significance level (fail to reject H_0);
* as digitised from Fig. 5 in Schmidt [75].

The distribution of resistances χ within each λ-bin is often skewed, with specimens in the intermediate slenderness range of $1.0 < \lambda < 1.75$ exhibiting the most pronounced levels of right-skew. In this range, the specimen buckling resistances are concentrated *below* the overall λ-bin mean, suggesting that it is unconservative to assume that these follow a classical symmetric normal distribution. With one significant exception (the λ-bin at 1.50 ± 0.125), the specimen buckling resistances usually exhibit a distribution that is 'flatter' than an equivalent normal distribution with potentially less weight in the tails (negative excess kurtosis). Indeed, three non-parametric tests for normality carried out with Matlab R2021a (the Anderson-Darling test, the Lilliefors test and the Shapiro-Wilk / Francia test, as coded by Ben Saïda [80]) revealed that the null hypothesis that the samples are normally distributed should be rejected at the 5% significance level for many of the λ-bins (Table 2). However, these conclusions should be treated with caution since the sample sizes are relatively small.

The newly compiled dataset for isotropic metal cylinders under uniform axial compression was next compared with the German dataset. The source used here for the German dataset is the figure described as the 'reliable' tests from a larger 1200-strong dataset and is said to consist of approximately 750 specimens [24,55,75]. This figure was digitised, and as many points as possible were identified through visual inspection. Whilst this is an unsatisfactory process, it could not be avoided since the original dataset is irrecoverable. Although this dataset was said to contain 750 results, only 366 could be confidently recovered due to the poor resolution and congestion of data in the source image, particularly for low slendernesses. The recovered dataset is illustrated in Fig. 2b.

Three two-sample non-parametric equality of distribution tests (the Kolmogorov-Smirnov test, the Mann-Whitney-Wilcoxon test and the Kruskal-Wallis test) were subsequently carried out in Matlab R2021. As shown in Table 2, these tests suggest that, for many of the intermediate slenderness λ-bins, the null hypothesis H_0 that the samples originate from the same population cannot be rejected at the 5% significance level (that is, it is 95% likely that they are originate from the same population). However, the two datasets appear to differ significantly in the low-slenderness λ-bins (this may also be seen in Fig. 2) where the resistance is dominated by plastic collapse and extensive strain hardening. This is partly because the present dataset included an additional series of 50 tests by Osgood [81] from 1938 which exhibited high resistances with $\chi > 1$, and partly because some of the German dataset could not be

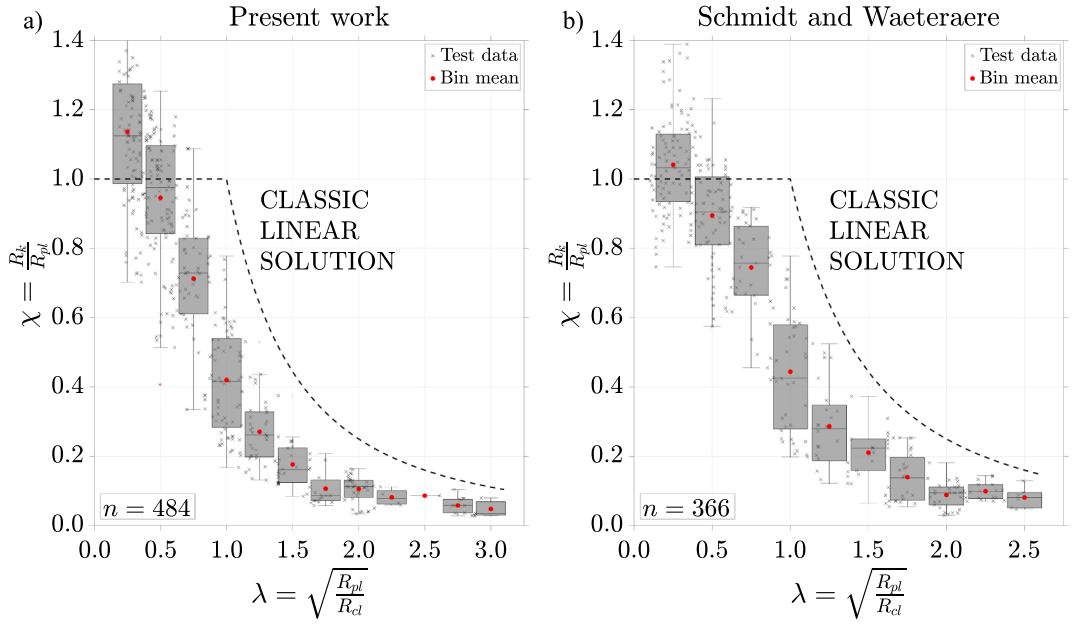


Fig. 2. Box-and-whisker summary of χ against λ for the dataset collected as part of the present work (a) and the German dataset (b), as digitised from Schmidt [75].

Table 3
Summary of 648 specimens according to fabrication category.

	Circular hollow section	Circ. & long. joined	Machined	Long. butt-joined	Long. overlap-joined	Electro-forming	Misc.
# Total	78 (12.0%)	36 (5.6%)	97 (15.0%)	99 (15.3%)	262 (40.4%)	46 (7.1%)	30 (4.6%)
Year	Earliest: 1909	1933	1933	1928	1933	1962	1933
	Median: 1938	1937	1950	1977	1939	1968	1959
	Latest: 2020	2016	1985	2017	2016	1972	2019
Radius (mm)	Min: 12.7	153.2	17.6	41.3	23.9	36.8	31.8
	Median: 25.4	280.0	46.3	150.0	161.9	75.6	64.0
	Max: 82.2	1016.0	173.6	893.4	381.3	102.7	762.0
Thickness (mm)	Min: 0.32	1.6	0.079	0.094	0.049	0.038	0.075
	Median: 1.5	6.2	0.61	0.79	0.15	0.090	0.77
	Max: 9.9	12.5	4.4	9.9	2.0	0.13	2.1
Length (mm)	Min: 50.8	1200.0	6.4	7.4	5.3	175.3	101.6
	Median: 139.8	9144.0	101.6	350.0	190.5	203.2	532.0
	Max: 505.3	11000.0	508.0	3050.0	812.8	254.0	2537.0
r/t ratio	Min: 6.6	24.0	4.5	24.5	37.5	363.3	30.3
	Median: 23.7	53.8	76.9	160.8	750.0	844.5	200.5
	Max: 49.7	172.1	763.4	666.7	3187.5	1160.0	990.1
Ω	Min: 0.11	0.14	0.017	0.0066	0.00064	0.055	0.032
	Median: 0.53	2.9	0.30	0.19	0.051	0.12	0.23
	Max: 2.5	11.8	3.7	1.9	2.5	0.29	3.4
λ	Min: 0.18	0.22	0.24	0.25	0.25	2.61	0.94
	Median: 0.29	0.34	0.56	0.59	1.30	2.76	1.30
	Max: 0.57	0.61	1.95	1.53	2.88	2.93	1.58
χ	Min: 0.92	0.51	0.046	0.15	0.029	0.057	0.085
	Median: 1.18	0.77	0.98	0.79	0.21	0.078	0.16
	Max: 1.76	1.12	1.31	1.15	1.11	0.10	0.59
α	Min: 0.041	0.044	0.062	0.065	0.069	0.43	0.074
	Median: 0.11	0.088	0.29	0.30	0.33	0.69	0.23
	Max: 0.32	0.26	0.74	0.84	1.60	0.96	0.87
# Aluminium	28 (35.9%)	0	59 (60.8%)	0	58 (22.1%)	0	8 (26.7%)
# Steel	50 (64.1%)	36 (100%)	38 (39.2%)	93 (93.9%)	174 (66.4%)	0	14 (46.7%)
# Copper	0	0	0	0	0	16 (34.8%)	0
# Brass	0	0	0	6 (6.1%)	30 (11.5%)	0	8 (26.7%)
# Nickel	0	0	0	0	0	30 (65.2%)	0

digitised in this region. Overall, the Authors assert that the presently compiled dataset may in future be treated as an ersatz to the German dataset if so desired, particularly in the range of intermediate to high slendernesses where failure is by elastic–plastic or elastic shell buckling.

4.3. Specimen fabrication summary

As stated above, six broad specimen fabrication categories were identified in the present dataset, with a seventh 'miscellaneous' category for specimens where the fabrication was less clear or formed a small group. A detailed break-down of the dataset by category is presented in Table 3 in terms of increasing median λ. For presentation purposes only, the numbers in this table are reported to two significant figures if they are less than unity and to one decimal point if they are greater than unity (except for λ, χ and α which are simply reported to at least two decimal points due to their limited scale), but no claim is made for the precision of these measurements as this is unknowable. The year refers to the year of publication of the source reference, with all tests performed as part of that study attributed the same year to permit the calculation of a median value. The earliest tests date from 1909 and the most recent from 2020 with 50% and 80% of all tests carried out before 1939 and 1971 respectively, suggesting an already very old dataset.

The stockiest specimens were either manufactured circular hollow sections (CHS), specimens fabricated out of panels with longitudinal and circumferential welds or machined out of larger pieces of metal. CHS are commercially manufactured in mills and thus conform to tight tolerance requirements, while machining similarly produces accurate geometries. Two categories with many tests were for specimens fabricated by joining together the ends of a thin sheet of material which was cold-rolled to the required curvature in the laboratory. These longitudinal joints were made by soldering or TIG-welding the butted ends of the curved sheets together directly (here termed 'butt-joined') or alternatively by forming a finite glued overlap (here termed 'overlap-joined'). The latter formed the largest single subset of specimens (262 out of 648, or 40.4%) and spanned the largest slenderness range of $0.25 < \lambda < 2.88$ or $37.5 < r/t < 3187.5$. For this reason, this group of longitudinally overlap-joined specimens will be the focus of the Monte Carlo simulations presented later in this paper.

The unfeasibly high maximum reported strength of $\alpha = 1.60$ (that is, buckling at 60% *above* R_{cl}) seen in this fabrication category (Table 3) came from the student test programme of Kanemitsu and Nojima [82] from 1939 who made very small steel specimens with a radius of 160 mm and as short as 6 mm high. Of the remaining specimens, 46 were fabricated through electroforming, a specialised procedure involving the electrodeposition of metal on a solid mandrel of circular cross-section, first used to create very high-quality metal shells in the 1960s [4,16]. Electroformed specimens are invariably slender, with $2.6 < \lambda < 3$ or $363 < r/t < 1160$, with the median specimen achieving a high normalised resistance α of almost 70% of R_{cl}.

4.4. Absolute scale

The classical representation of the dataset on a capacity relationship between a dimensionless resistance and a dimensionless geometry masks

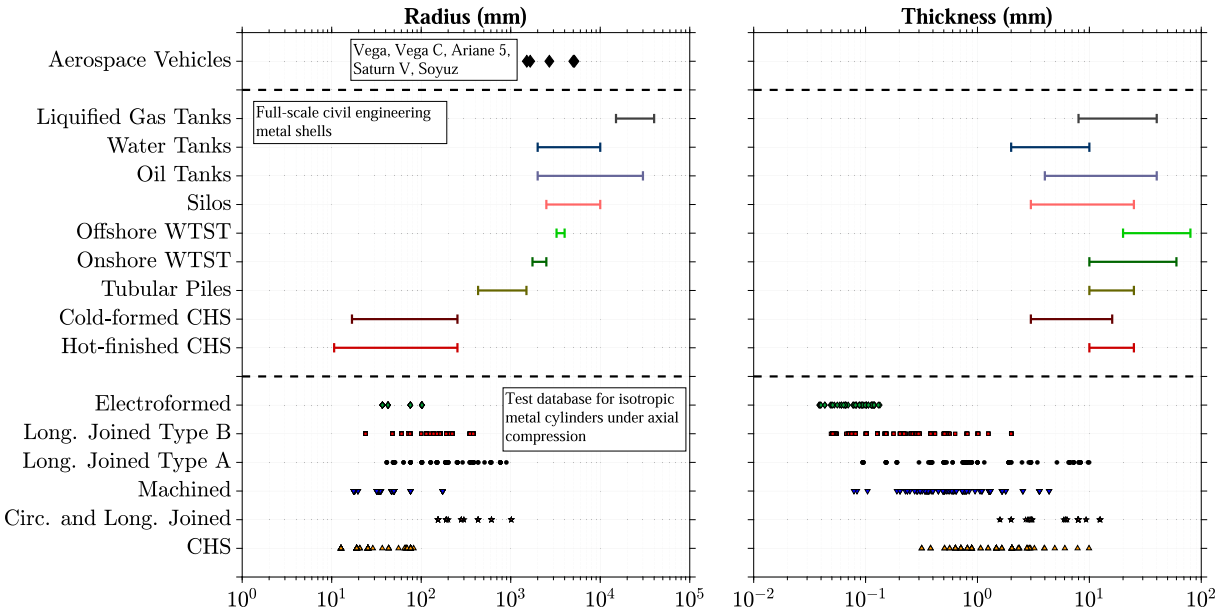


Fig. 3. Illustration of order of magnitude scale differences between the radii and thicknesses of tested specimens and typical civil engineering applications of steel shells.

the absolute scale of the tested specimens. Illustrated in Fig. 3, the typical radius and thickness ranges of the six main categories of the present dataset are compared against approximate ranges of the same for various civil engineering metal shell applications (the radii for aerospace vehicles are also shown for comparison, simple thicknesses not being available for these complex stiffened shells). The full-scale geometries were compiled on the basis of commercial material [83–85] and the Authors' professional experience. The test data are only for isotropic cylindrical metal shells under uniform axial compression, but similar figures could be constructed for the other fundamental load cases of uniform external pressure and torsion and for other geometries such as conical or spherical shells. As stated in the Introduction, the absolute geometric scale of the stockiest CHS specimens corresponds quite closely to those of commercial CHS members used in construction (although the tested specimens are still frequently thinner than the commercial product), thus broadly supporting their use as a basis for calibration of design resistance equations. By contrast, most full-scale civil engineering shell applications lie between two and three orders of magnitude larger than the tested specimens in both radius and thickness. With such large differences of absolute scale, the use of small-scale laboratory tests as a basis for design calibration is very difficult to justify.

5. Postulated imperfections in longitudinally joined specimens

The midsurface geometry and loading conditions of the tests in the above dataset are unknowable, making it difficult to achieve a direct reproduction of the buckling resistances with finite element analysis. Instead, the remainder of this study illustrates how a synthetic dataset with similar statistical characteristics as the observed one may be generated using Monte Carlo simulation and postulated imperfections based on reasonable assumptions regarding the conditions that may have existed during a test. For the first ever time, such an exercise will generate information to permit an approximate yet direct quantitative assessment of the quality of the tested specimens that form the present observed 'legacy' test dataset. In turn, this will allow the scientific community to assess the representativeness of this dataset of full-scale civil engineering construction, and to conclude with justification whether or not it is an appropriate basis for calibration of their safety margins. The reproduction is restricted to the subset of 262 longitudinally overlap-joined cylinders, which constitute the largest group and 40% of the tested specimens, where the rolled plate is first made to overlap by an angle θ_0 prior to welding, soldering or gluing. Butt-welding is unfeasible for thinner specimens.

The longitudinal joint is treated as a region of local flattening whose stiff overlapped double-thickness imposes strict circumferential continuity requirements on the geometry of the shell midsurface that are manifested as a systematic out-of-roundness imperfection, shown exaggerated in Fig. 4a. In polar coordinates, the postulated geometry of the shell midsurface position ρ as a function of the circumferential coordinate θ in the range $0 \leq \theta \leq \pi$ may be defined as:

$$\rho_B(\theta) = \begin{cases} \rho_F(\theta) & |\theta| \leqslant \theta_0 \\ \rho_C(\theta) & |\theta| > \theta_0 \end{cases} \tag{3}$$

where ρ_F and ρ_C represent the 'flat' and 'curved' portions of the shell circumference and are respectively defined as:

$$\rho_F(\theta) = \frac{r - \delta_0}{\cos\theta} \text{ and } \rho_C(\theta) = r - e^{\left(a_1\theta^3 + a_2\theta^2 + a_3\theta + a_4\right)} \cos 2\theta \tag{4}$$

In addition to the radius of the nominal (perfect) cylinder r, six parameters must be supplied to generate a unique imperfect shell geometry:

- θ_0, the angular circumferential extent of the 'joint' region;
- δ_0, a 'reference' amplitude of the inwards radial deviation at the joint midline;
- a_1, a_2, a_3 and a_4; exponents governing the curvature of the 'curved' shell portion.

Both the radius r and the angle θ_0 were treated as random variables sampled from empirically constructed probability distributions based on the reconstructed dataset, with θ_0 deduced from reported information on the width of the overlap, leaving five unknown parameters. The reference amplitude δ_0 may be found by minimising the out-of-roundness of the constrained imperfect geometry, represented in M1 below by the square root of the integral of the squared difference between the varying circumferential curvature of the imperfect geometry $\kappa(\theta)$ and the constant

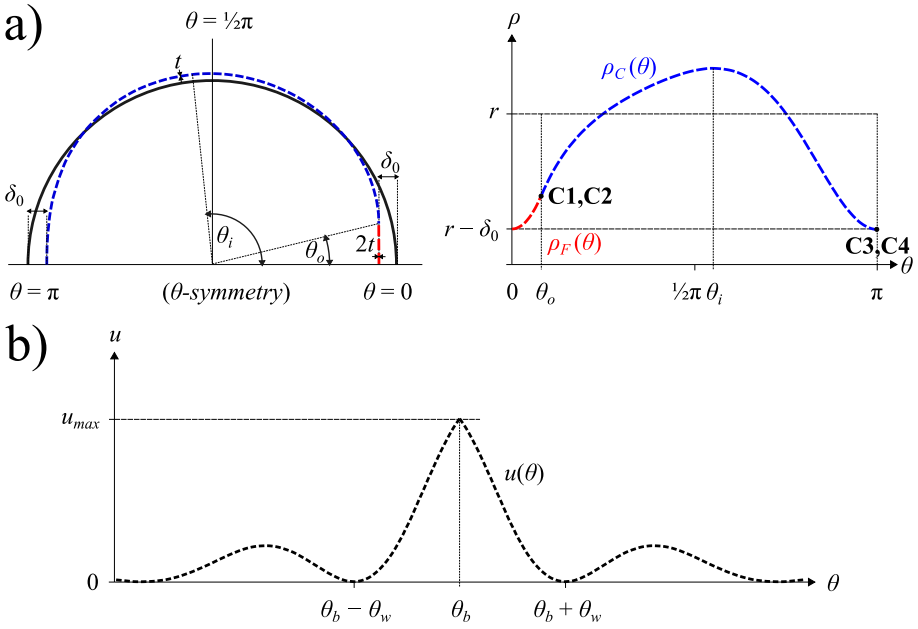


Fig. 4. Postulated a) geometric imperfection with a longitudinally overlap-joined specimen and b) load application non-uniformity.

circumferential curvature of the nominally perfect geometry ($1/r$). This condition is a proxy for the bending strain energy of the shell, which the fabricated geometry will naturally minimise in a state of static equilibrium. The imposed out-of-roundness is, for simplicity, treated as symmetric about the plane passing through $\theta = 0$ and π, though it is recognised that a material overlap would induce a slight circumferential asymmetry. The angle θ_i identifies the position of the peak most outward deviation and location of highest circumferential curvature, usually occurring close to ½π. The flattest region of the curved portion of the circumference occurs at $\theta = \pi$ where, due to the increased local circumferential radius of curvature, premature buckling failure is likely ($R_{cl} / (2\pi rt) \to 0$ as $r \to \infty$).

$$\boldsymbol{M1}: \text{minimise}\left(\sqrt{\int_0^{\pi}\left(\kappa(\theta)-\frac{1}{r}\right)^2 d\theta}\right)$$

$$\text{where } \kappa(\theta) = \frac{\left|\rho(\theta)^2 + 2\left(\frac{d\rho}{d\theta}\right)^2 - \rho(\theta)\frac{d^2\rho}{d\theta^2}\right|}{\left(\rho(\theta)^2 + \left(\frac{d\rho}{d\theta}\right)^2\right)^{\frac{3}{2}}} \tag{5}$$

For each trial value of δ_0, the remaining four coefficients a_1, a_2, a_3 and a_4 may be obtained by least-squares fitting to satisfy the four geometric constraints:

$$\boldsymbol{C1}: \text{continuity of the shell midsurface at } \theta_0 : \rho_F(\theta_0) = \rho_C(\theta_0) \tag{6}$$

$$\boldsymbol{C2}: \text{continuity of the circumferential midsurface gradient at } \theta_0 : \left.\frac{d\rho_F}{d\theta}\right|_{\theta=\theta_0} = \left.\frac{d\rho_C}{d\theta}\right|_{\theta=\theta_0} \tag{7}$$

$$\boldsymbol{C3}: \text{plane of circumferential symmetry at } \theta = \pi : \left.\frac{d\rho_C}{d\theta}\right|_{\theta=\pi} = 0 \tag{8}$$

$$\boldsymbol{C4}: \text{enforced radially outward deviation at } \theta = \pi : \rho_C(\pi) = r - \delta_0 \tag{9}$$

The postulated form of the load application non-uniformity involves a deviation from perfect flatness of the base shell boundary, achieved via an enforced circumferentially varying pre-buckling displacement in the axial direction $u(\theta)$ of the form [95]:

$$u(\theta) = \frac{u_{\max}}{2}\left[1 + \cos\left((\theta-\theta_b)\frac{\pi}{\theta_w}\right)\right] \quad \text{if } \theta_b - \theta_w \leqslant \theta \leqslant \theta_b + \theta_w \text{ (elsewhere zero)} \tag{10}$$

where $u_{\max} = 2\beta\theta_w r/\pi$, θ_b and θ_w represent the location of the peak flatness deviation and the circumferential angular half-width of each wave of the deviation respectively, while $u_{\max}$ represents the deviation's peak amplitude (Fig. 4b). This enforced $u(\theta)$ field has the property that its maximum gradient in the circumferential direction is:

$$\left|\frac{du}{ds}\right|_{\max} = \left|\frac{1}{r}\frac{du}{d\theta}\right|_{\max} = \beta \tag{11}$$

where here β may be interpreted as the 'interface flatness tolerance' of EN 1993–1-6 [54], specifically the 2007 version. The prescribed deterministic limiting value is just $0.1\% = 10^{-3}$ rad, which for a specimen with a nominal radius of $r = 161.9$ mm (the median value for longitudinally overlap-joined specimens, see Table 3) and a relatively wide half-spread angle of $\theta_w = ¼\pi$ corresponds to a peak flatness deviation amplitude of an almost imperceptible $u_{\max} = ½\beta r \approx 81$ μm, an imperfection that could very easily arise in a typical laboratory test and would scarcely have been controlled for in the past.

6. Finite element implementation

The postulated imperfections just presented were implemented in general shell finite element models for arbitrary nominal geometries for use in the Monte Carlo simulations described shortly, performed using the ABAQUS 2020 [86] commercial software. For efficiency, symmetry conditions were used to model only half of the shell circumference. The half-circumference was calculated according to $\rho(\theta)$ in Eq. (3) and then extruded to the desired length L to create a continuous 3D shell midsurface. Two reference points were created at the centroid of the nominal geometry at either end of the cylinder, shown in Fig. 5. These were then linked kinematically to their respective edge, such that all degrees of freedom (*dofs*) on that edge were constrained to be that of the reference point. The top reference point at $z = L$ was loaded by a point force of magnitude $½R_{cl}$ (due to symmetry, see Eqs (1) & (2)) and permitted to displace only in the meridional z direction, with all other displacement Δ and rotation β *dofs* restrained to zero. The bottom reference point at

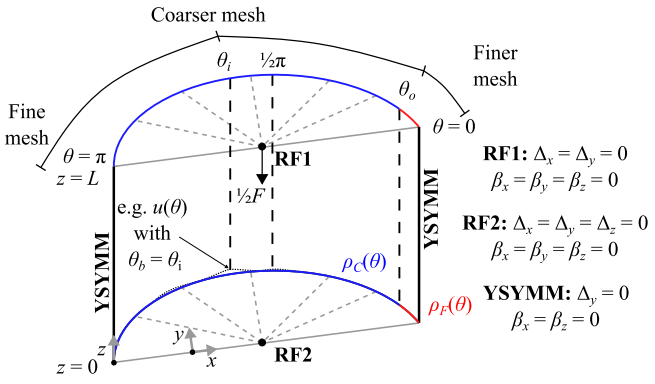


Fig. 5. General finite element model template.

$z = 0$ was restrained against all movement. Specifically to isolate the effect of out-of-roundness, the choices were made to not enforce cross-sectional circularity at the loaded supports in the test arrangement and to use idealised boundary conditions elsewhere in the model.

Linear shell bending theory and Koiter circle linear bifurcation buckling theory [87–88] were used to design a scalable mesh refinement based on the geometry of the nominal perfect cylinder. The Koiter circle predicts the smallest possible meridional Λ_z and circumferential Λ_θ half-wavelengths that a linear buckling eigenmode can exhibit under uniform axial compression as:

$$\Lambda_z = \frac{\pi}{[12(1-\nu^2)]^{1/4}}\sqrt{rt},\ \Lambda_\theta = 2\Lambda_z \text{ and } \Lambda_b = \sqrt{2}\Lambda_z \tag{12}$$

A widely used 'rule of thumb' [89–91] suggests that a finite element mesh is considered sufficiently fine for buckling analyses in thin shells involving stress states dominated by axial compression when the element size is not larger than 1/10 of the smallest possible half-wavelength along a particular axis. For additional efficiency, and because buckling would always be localised where the imperfect shell wall was circumferentially flattest, circumferentially graded meshing was used. The chosen circumferential element size was Λ_θ / 15 in the vicinity of $\theta = \pi$ and θ_0, but since buckling deformations were unlikely elsewhere due to the higher circumferential curvature, the mesh could be significantly coarser (up to $2\Lambda_\theta$ / 3), as illustrated in Fig. 5. The element size in the z direction was kept uniformly fine at Λ_z / 15, thus also enabling an accurate representation of the local compatibility bending near the shell edges whose half-wavelength $\Lambda_b > \Lambda_z$. The four-node reduced-integration bilinear S4R shell element was employed, which is widely used in shell buckling studies of this nature (see discussion in Section 4.3 of Wang *et al.* [92]). It is stressed that the discussion above concerns a meshing protocol for relatively thin shells where highly localised buckling is anticipated. Thicker shells whose response is dominated by plasticity may not require such high mesh refinement.

Two computational analyses were performed for each generated out-of-round geometry: a linear bifurcation analysis of the imperfect shell (LBIA) and a geometrically and materially nonlinear analysis (GMNIA),

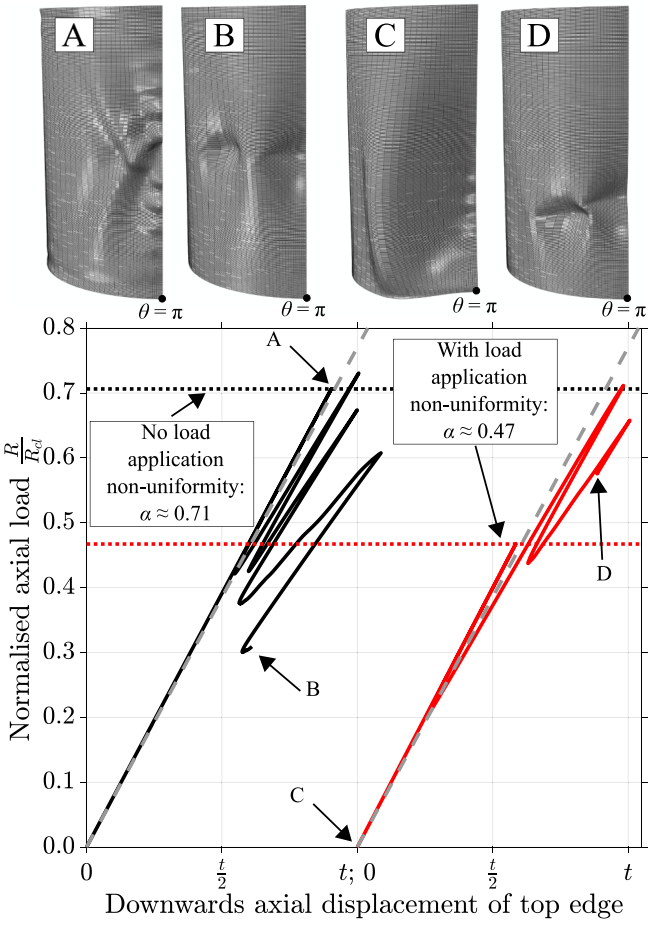


Fig. 6. Illustration of a typical GMNIA simulation result (equilibrium paths, incremental buckling modes A and deformed shapes B, C & D) for a representative 'median' cylinder specimen with and without load application non-uniformity.

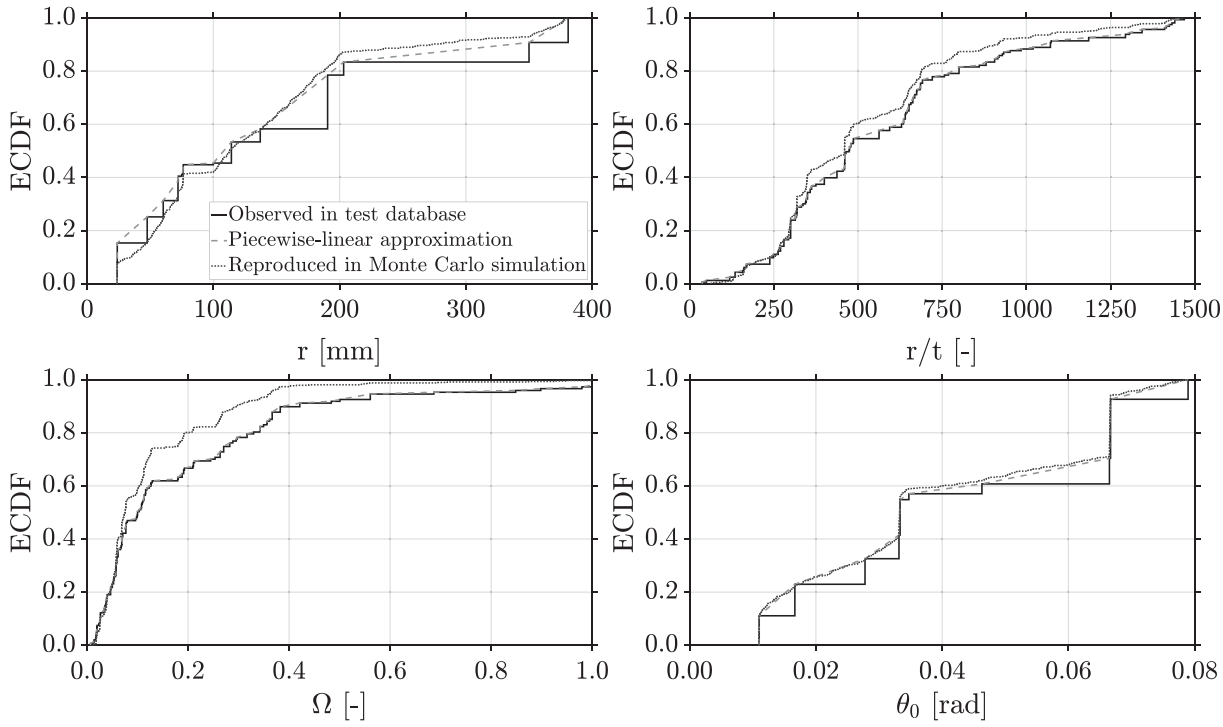


Fig. 7. Actual, piecewise approximated and sampled empirical cumulative distribution functions (ECDFs) adopted for the Monte Carlo simulation of specimens with longitudinally overlap-joined systematic fabrication imperfection.

also using the out-of-round imperfect geometry (the 'I') as defined in Section 5. The sole aim of the LBIA was to generate an eigenmode geometry that could act as a small (peak-to-peak amplitude of 0.02 t) mesh perturbation to trigger a bifurcation in the out-of-round GMNIA, ideally on the 'flattest' curved portion at $\theta = \pi$. Where a pre-buckling axial displacement was used to model load application non-uniformity, this was applied in a separate nonlinear analysis step as part of a two-step GMNIA. The nonlinear buckling load was always obtained using the Riks [93] modified arc-length algorithm. Generation, submission, termination and processing of the models was automated using the methodology of Sadowski *et al.* [94], an open-source publication which the reader is invited to consult for a detailed discussion of the adopted buckling criteria. A simple bilinear elastic–plastic material model with no strain hardening was assumed, with choices of material properties defined below. For the chosen geometries, the majority of longitudinally joined specimens would be expected to buckle elastically during experiments ($\alpha = R_k / R_{cl} < 1$ and $R_{cl} < R_{pl}$), and any local yielding leading to strain hardening is unlikely to have a significant effect on the buckling event. For the same reason, it was deemed unnecessary to model nonlinear stress–strain curves that are characteristic of nickel, brass, copper and aluminium, though these metals were used in some of the tests.

An illustration of a typical GMNIA simulation is presented in Fig. 6 for a model representing an approximately 'median' (see Fig. 7) longitudinally joined medium length cylinder with a nominal $r = 112$ mm, $t = 0.243$ mm ($r/t \approx 460$), $h = 240.2$ mm ($\Omega \approx 0.1$), $E = 210$ GPa and $f_y = 355$ MPa. An imperfect geometry was generated using Eq. (3) that is at the limit of out-of-roundness for Fabrication Tolerance Quality Class A ('excellent') as defined in Section 8.4.2 of EN 1993–1-6 [54,58] where the out-of-roundness tolerance is represented by the parameter $U_r = (d_{max} - d_{min}) / d_{nom}$, with d_{max}, d_{min} and d_{nom} representing the maximum, minimum 'measured' and nominal internal diameters respectively. The 'measured' value should be less than a limiting value $U_{r,max}$ which is defined as $U_{r,max} = 0.014$, 0.02 or 0.03 for Fabrication Tolerance Quality Classes A ('excellent'), B ('very good') or C ('normal') respectively. For the model without load application non-uniformity, the postulated out-of-roundness due solely to the longitudinal joining process was found to reduce the buckling load down to 71% of R_{cl}. The critical incremental buckling mode was a localised buckle at approximately midlength at $\theta = \pi$ (marked with 'A' in Fig. 6). This initial buckle spread around the circumference with each subsequent post-buckling bifurcation ('B'; ×7 scaling) leading to a buckling pattern consistent with observations in test programmes (see discussion in Section 9.2.1 of Singer *et al.* [4]). For the model with an additional load application non-uniformity as defined by Eq. (10), the additional imposed pre-buckling displacements in the axial direction $u(\theta)$ induced severe out-of-plane bending distortions in the shell wall throughout the specimen length ('C'; ×250 scaling) owing to the orders of magnitude difference between the high axial membrane stiffness and low circumferential bending stiffness of a cylindrical shell [88,95]. These distortions introduced local axial compressive stresses that reduced the load corresponding to the first buckling event to just 47% of R_{cl} and moved the buckle location slightly downwards ('D'; ×7 scaling). In what follows here, only the first buckling event is recorded since tracing the post-buckling equilibrium paths involves considerable computational complexity.

7. Monte Carlo simulation

7.1. Empirical probability distributions

The final part of this study employs Monte Carlo sampling together with GMNIA finite element analysis to synthetically recreate, in a statistical sense, the portion of the dataset of observed test results that involved longitudinally overlap-joined specimens (which occupy intermediate and high slenderness ranges). This exercise serves the important purpose of illustrating that such a purely computational recreation is possible in principle if the imperfect geometry of the shell is realistically defined. For the present tested specimens whose imperfections are

Table 4
Bootstrapped hypothesis testing (10,000 resamples) comparing descriptive statistics of the present test dataset with that of the German dataset expressed as p values per statistic and λ-bin (H_0: samples come from a population sharing that statistic).

$\lambda_i \pm 0.125$ bin	Percentile			Mean	Standard deviation	Skew	Excess kurtosis	Sample sizes	
	5^{th}	50^{th} (median)	95^{th}					Present work	German dataset‡
0.25	**0.19**†	0.0051	**0.011**	0.0040	<0.001	**0.94**	**0.75**	103	99
0.50	**0.27**	0.046	**0.018**	0.046	0.010	**0.11**	**0.74**	122	75
0.75	**0.17**	**0.44**	**0.34**	**0.36**	**0.092**	**0.69**	**0.41**	54	35
1.00	**0.62**	**0.75**	**0.85**	**0.45**	**0.29**	**0.54**	**0.28**	68	40
1.25	**0.48**	**0.60**	**0.19**	**0.56**	**0.13**	**0.68**	**0.32**	36	24
1.50	**0.51**	**0.067**	**0.37**	**0.11**	**0.51**	**0.078**	**0.16**	25	18
1.75	**0.89**	**0.16**	**0.061**	**0.081**	**0.062**	**0.25**	**0.34**	19	23
2.00	**0.21**	**0.080**	**0.16**	**0.069**	**0.76**	**0.052**	**0.38**	36	30
2.25	**0.34**	**0.27**	**0.23**	**0.21**	**0.91**	**0.80**	**0.50**	4	16

† p values greater than 0.05 indicate that samples from the present test dataset and those from the German dataset in the given λ-bin are likely to have originated from a population that shares that statistic at the 5% significance level (fail to reject H_0);
‡ as digitised from Fig. 5 in Schmidt [75].

unfortunately now unknowable, the realism of the imperfect geometry comes from the purposeful imperfection models presented in Section 5. As will be argued after, a similar procedure can in principle be applied to full-scale civil engineering shells if their imperfect midsurface geometry can be sampled by optical scanning or other means, although this may need to be supplemented with auxiliary information relating to residual stresses or other material defects.

Empirical cumulative distribution functions (ECDFs) for the nominal cylinder radius r, r/t ratio and dimensionless length $\Omega = (L/r)\sqrt{(t/r)}$ were first constructed in a piecewise linear fashion from the accumulated dataset from which pseudo-populations of r, t and L could be randomly sampled (see Fig. 7). Sampling t and L directly from their own ECDFs was avoided as this was found to lead to r/t and Ω distributions that were unrepresentative of the dataset due to non-negligible correlations between these variables. Only 163 tests out of the total of 262 for this fabrication category for which a yield stress and tested buckling load were available were used in the construction of the ECDFs and in the comparisons which follow. This restriction had the additional advantage that it removed some of the more contentious data from the comparison, such as the numerous very small specimens of Kanemitsu and Nojima [82]. Once a (r, t, L) triplet was established, the angle θ_0 was randomly sampled from a piecewise ECDF constructed on the basis of reported material overlaps and used to generate a systematically imperfect geometry according to the procedure presented in Section 5 (Fig. 7). From a target sample of 1000 imperfect geometries devised as described above, the strict circumferential continuity constraints imposed by C1 to C4, as well as further requirements that each shell's thickness and length established from a sampled r, r/t and Ω remained within the bounds exhibited by the dataset for this cluster and that an LBIA triggers buckling away from the joint, led to only ~560 feasible geometries for GMNIA.

For each successfully generated geometry, a nominal material was selected with a probability based on that material's frequency of occurrence in the subset of the test dataset for the chosen fabrication form containing tests for which all material properties were available. The model thus had a 33.7%, 47.9% or 18.4% chance of representing an aluminium, steel or brass specimen respectively (by contrast with Table 3 which also includes tests with no reported no yield stress). Once a material has been selected, an elastic modulus E was randomly sampled from an ECDF constructed on the basis of all reported moduli in the dataset for that material and this imperfection type. The yield stress f_y was taken from the specimen whose E value was drawn in the above manner, thus preserving realistic E-f_y material pairs, and used to define an ideal elastic–rigid plastic bilinear material law with no strain hardening. Poisson's ratio was taken as $\nu = 0.3$ for all metals. Finite element models were then generated and executed as described in Section 6. Each generated imperfect geometry was additionally assessed against the out-of-roundness tolerance requirement of Section 8.4.2 in EN 1993–1-6 [54].

7.2. Bootstrapped hypothesis testing procedure

Bootstrapping is a purely computational non-parametric procedure to generate sampling distributions for any statistic for which classical parametric sampling distributions (e.g. normal, Student's t, χ^2 or F) are either not known or their use cannot be justified [96]. Statistics with unknown sampling distributions include those based on ordered data rankings such as a median or a percentile, while classical sampling distributions for unordered statistics such as the mean or standard deviation were considered unjustifiable for the present data because it may not satisfy the important prerequisite of simple random sampling [97]. Assuming two independent samples of buckling resistances $X = \{x_1, \ldots, x_n\}$ of size n and $Y = \{y_1, \ldots, y_m\}$ of size m and a null hypothesis (H_0) that they both come from a population that shares the same summary statistic (e.g. mean, median, standard deviation etc.), the adopted procedure for bootstrapped two-sample testing of H_0 is as follows (Algorithm 16.1 in Efron & Tibshirani [98]):

- Compute a single observed 'difference of' test statistic $TS = f(X) - f(Y)$, where $f()$ is a function to compute any desired summary statistic;
- Combine both samples into a single sample $Z = \{x_1, \ldots, x_n, y_1, \ldots, y_m\}$ of size $n + m$ under the assumption that H_0 is true;
- Draw a 'resample with replacement' from Z of size $n + m$, of which the first n observations identify a set X* and the remaining m identify a set Y*;
- Compute a bootstrapped 'difference of' test statistic $TS^* = f(X^*) - f(Y^*)$ for that resample;
- Repeat the resampling procedure $B = 10{,}000$ times and construct a bootstrapped sampling distribution TS_B^* of the 'difference of' test statistic;

The two-tailed p value, or the probability of observing the 'difference of' test statistic TS assuming the null hypothesis H_0 is true, is computed as:

$$p = \frac{\#\{TS_B^* \leqslant -|TS|\}}{B} + \frac{\#\{TS_B^* \geqslant |TS|\}}{B} \tag{13}$$

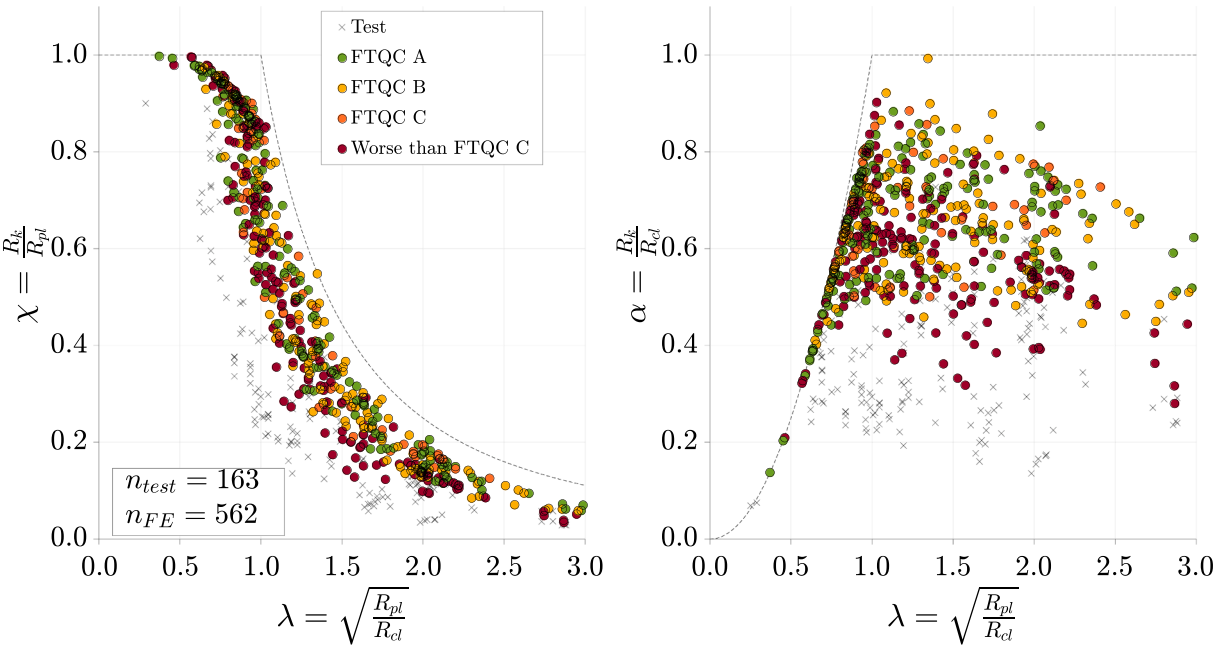


Fig. 8. Collected test vs synthetic Monte Carlo datasets for χ and α against λ for test specimens with a longitudinally overlap-joined systematic fabrication imperfection.

Table 5
Bootstrapped hypothesis testing (10,000 resamples) comparing descriptive statistics of the present test dataset of longitudinally overlap-joined specimens with a synthetic version of this dataset generated by Monte Carlo simulation expressed as p values per statistic and λ-bin with a sufficient number of samples (H_0: samples come from a population sharing that statistic).

$\lambda_i \pm 0.125$ bin	Percentile			Mean	Standard deviation	Skew	Excess kurtosis	Sample sizes	
	5th	50th (median)	95th					Lab specimens	Monte Carlo FE
0.75	0.0029	<0.001	<0.001	<0.001	0.0036	**0.054**	**0.24**	26	87
1	0.0097	<0.001	<0.001	<0.001	**0.42**	<0.001	**0.34**	30	152
1.25	<0.001	<0.001	<0.001	<0.001	**0.091**	**0.38**	**0.16**	27	94
1.5	**0.064**	0.017	**0.48**	<0.001	**0.68**	**0.15**	**0.46**	12	57
1.75	0.0025	<0.001	<0.001	<0.001	**0.83**	0.0020	**0.32**	18	46
2	0.0040	<0.001	0.0055	<0.001	**0.084**	**0.096**	**0.84**	34	66

† p values greater than 0.05 indicate that samples from the present test dataset and those from the synthetic one in the given λ-bin are likely to have originated from a population that shares that statistic at the 5% significance level (fail to reject H_0).

where # represents the number of occurrences of TS_B* that satisfy the condition in the curly brackets. A conventional significance level of 5% was used, with H_0 rejected when $p \leq 0.05$. The Authors had additionally performed permutation tests and hypothesis testing based on variously bootstrapped confidence intervals which included bias correction, as well as non-parametric equality of distribution previously introduced in Table 2. The results of these additional tests are not presented here due to space limitations, but they led to conclusions consistent with those of the bootstrapping procedure presented above.

By way of illustration, the above procedure was first applied to statistically compare the current new compiled dataset of tested isotropic cylinders under uniform axial compression against the German dataset up to and including the λ-bin for $\lambda = 2.25$ (insufficient sample size for higher λ). Seven bootstrapped sample statistics were compared per λ-bin: the 5th, 50th (median) and 95th percentiles, and the mean, standard deviation, skew and excess kurtosis. The fewer the summary statistics for which H_0 fails to be rejected, the more credible it is that the two samples being compared come from the same population. As presented in Table 4, the bootstrapped hypothesis testing leads to similar qualitative conclusions to those shown previously in Table 2 (i.e. that the two datasets are statistically similar, except in the two lowest slenderness λ-bins for which reasons have already been given). However, this bootstrapped treatment provides more detail that gives a better understanding of the differences between the two datasets than is possible from equality of distribution tests alone.

7.3. Synthetic dataset for longitudinally overlap-joined specimens

The results of the first Monte Carlo simulations attempting to synthetically reproduce the collected test dataset for the longitudinally overlap-joined specimens are presented in Fig. 8 as χ vs λ and α vs λ capacity relationships. These simulations considered *only* the out-of-roundness imposed by the postulated systematic imperfections corresponding to the longitudinal joining fabrication process, with no dimples or load application non-uniformities. Comparisons between the simulations and the actual test data via bootstrapped hypothesis testing are presented in Table 5. The observed and simulated datasets are similarly dense in different regions of λ, pointing to a representative Monte Carlo sampling procedure.

The synthetic dataset suggests that many of the original specimens

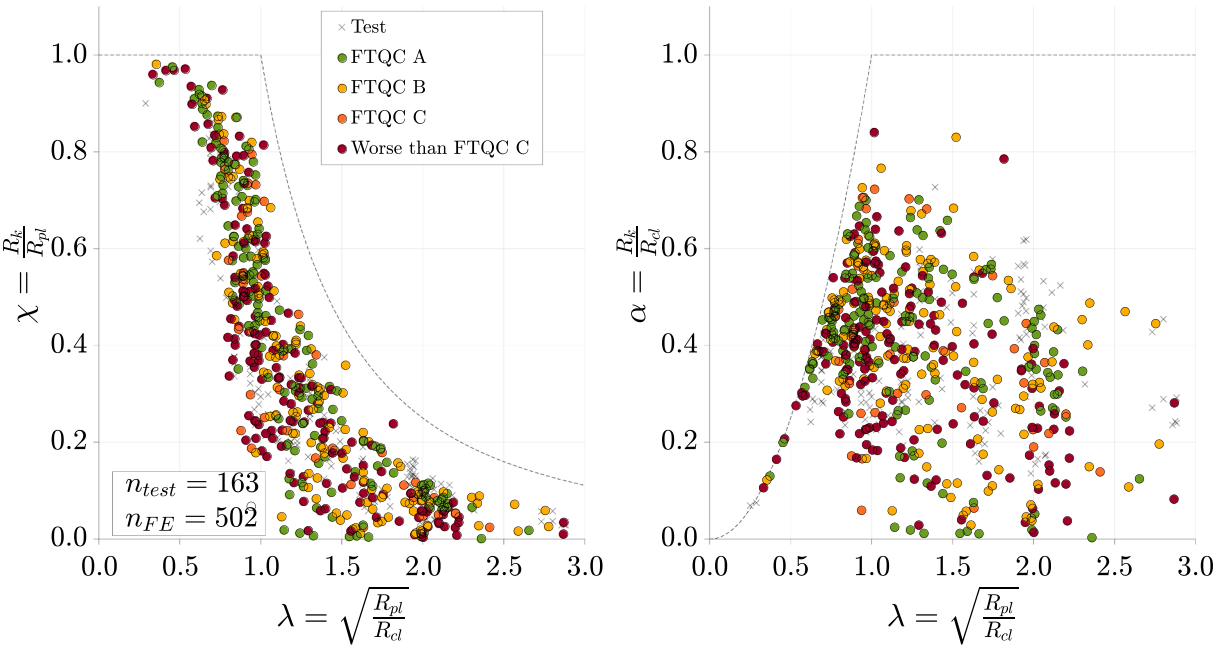


Fig. 9. Collected test vs synthetic Monte Carlo datasets for χ and α against λ for test specimens with a longitudinally overlap-joined systematic fabrication imperfection and an imposed deterministic load application non-uniformity.

Table 6
Bootstrapped hypothesis testing (10,000 resamples) comparing descriptive statistics of the present test dataset of longitudinally overlap-joined specimens with a synthetic version of this dataset generated by Monte Carlo simulation including load application non-uniformity expressed as p values per statistic and λ-bin with a sufficient number of samples (H_0: samples come from a population sharing that statistic).

$\lambda_i \pm 0.125$ bin	Percentile			Mean	Standard deviation	Skew	Excess kurtosis	Sample sizes		median reduction viz. Table 5‡
	5th	50th (median)	95th					Lab specimens	Monte Carlo FE	
0.75	**0.28**	**0.33**	**0.13**	**0.16**	**0.64**	**0.87**	**0.71**	26	87	18%
1.00	**0.90**	<0.001	0.0063	<0.001	0.010	0.0011	**0.17**	30	149	30%
1.25	0.016	**0.58**	0.014	**0.78**	<0.001	**0.32**	**0.47**	27	88	34%
1.50	0.036	**0.32**	**0.35**	**0.14**	**0.22**	**0.21**	**0.053**	12	44	36%
1.75	**0.064**	**0.19**	**0.50**	**0.34**	**0.095**	0.0063	**0.14**	18	38	48%
2.00	0.017	0.0020	<0.001	<0.001	**0.44**	**0.47**	**0.25**	34	54	49%

† p values greater than 0.05 indicate that samples from the present test dataset and those from the synthetic one in the given λ-bin are likely to have originated from a population that shares that statistic at the 5% significance level (fail to reject H_0);
‡ this is the % reduction in the median value of that λ-bin relative to the results without load application non-uniformity presented in Table 5.

may have been severely affected by the systematic out-of-roundness imperfection imposed by longitudinal lap-joining of material, and many would probably fail to qualify even as a FTQC Class C according to EN 1993-1-6 [54,58]. Although very severe, the imposed postulated out-of-roundness imperfection does not by itself appear to be capable of producing buckling resistances as low as those observed in the tests. For example, the lowest test result exhibited a normalised buckling load of $\alpha \approx 0.15$ or 15% of the classical elastic critical buckling stress R_{cl} at $\lambda \approx 2$, while the lowest simulated buckling load was about $\alpha \approx 0.35$. The two datasets exhibit similarly shaped distributions and scatter ($p > 0.05$ for standard deviation, skew and kurtosis for λ-bins with $\lambda \geq 1$), but significantly different centres of gravity ($p \leq 0.05$ for the mean and the percentiles).

7.4. Synthetic dataset including load application non-uniformity

The following results come from models with the same systematically out-of-round geometries as above, established on the basis of random sampling from the ECDFs in Fig. 7, but with the additional imposition of a postulated load application non-uniformity according to Eq. (10). Due to the complete absence of quantitative information on the load application non-uniformity in the compiled test dataset, the present treatment of this phenomenon can only be deterministic and thus advisory at best. A preliminary sensitivity study suggested that the influence of the imposed displacements $u(\theta)$ may be at its most damaging when the peak wave is centred at the region of lowest curvature ($\theta_i = \pi$) and is relatively wide (little further effect for $\theta_w > \sim¼\pi$). The enforced u_{max} was consistently of the order of tens of μm, an interface flatness deviation that would have been imperceptible during a test without exceptional attention on the part of the experimentalist.

The computed synthetic dataset is shown in Fig. 9 together with the test dataset. The effect of this form of imposed load application non-uniformity was found to be substantial, with the median resistance for each λ-bin suffering between ~18% and ~49% reduction, with a slight dependency on the slenderness. In 60 of the simulated geometries these imposed displacements were by themselves sufficient to cause instability in the first analysis step before an axial load was applied, and for this reason fewer simulation results are shown in Fig. 9 than in Fig. 8. The

reductions in buckling resistance are qualitatively consistent with (though perhaps more severe than) the experiments of Ummenhofer [22] who observed a pre-buckling axial stress deviation and amplification of between ~12% and ~27% relative to the mean axial membrane stress on axially-loaded metal specimens with r/t in the range ~660 to ~1120, despite careful attention to achieve a load application that was as uniform as possible. An even closer agreement between the synthetic and observed datasets is probably achievable if variations in the specimen thickness and material properties are additionally considered, but these are unknowable for these specimens.

The bootstrapped statistical comparison given in Table 6 suggests that the reduction in the computed resistances is now sufficient to make the two datasets statistically similar in both location and shape of the resistance distributions in the λ-bins centred at 0.75, 1.5 and 1.75 (confirmed by non-parametric equality of distribution tests, see Table 2), although elsewhere the agreement is less clear. This statistical affinity has been achieved here without recourse to the random dimple imperfections that are widely used in eigenmode shapes in computational imperfection sensitivity studies. Although it is likely that such dimples were present in the test specimens, they may not necessarily be the main source of test scatter and low buckling resistances. The above indicates that load application non-uniformity may therefore be an important confounding factor that has been imperceptibly present but never explicitly controlled for in all datasets of this nature. Anecdotal evidence indicates that Professor Maria Esslinger [99], who in 1970 published the results of many axial compression tests and was the first to use high speed photography to observe the buckling process, believed that loading non-uniformity alone accounts for 30% of the reduction in buckling resistance under axial compression.

8. Discussion

An extensive dataset of 648 historic buckling tests of cylindrical metal shells under uniform axial compression was collected, documented and analysed. It is clear that the specimens in this dataset were either constructed without any serious attempt to control their quality (because the importance of imperfection sensitivity was not yet appreciated), or conversely with the aim of making them as perfect as possible (e.g. manufactured by electroforming or to exhibit recoverable elastic behaviour through the use of mylar polymer). The aim of these historical test programmes was often to validate theories of mechanics rather than to establish representative databases for the purposes of calibration of design resistances relevant to full-scale civil engineering construction. Any temptation by the scientific community to use this dataset for such purposes just because it exists and is relatively populous should therefore be strongly resisted, and a similar caution should be issued for other apparently widely-tested fundamental shell systems such as cylindrical shells under uniform bending [92] or spherical shells under uniform external pressure [100].

It remains unfeasible to attempt destructive testing of full-scale metal shell structures such as wind turbine support towers, silos and tanks for the purposes of obtaining a statistically representative dataset upon which design resistance processes can be calibrated using probabilistically determined partial factors. Due to the obvious practical difficulties of performing such tests, datasets relating to full-scale shells may never be possible. This situation sets the modern subdiscipline of civil engineering shells apart from others within classical structural engineering, where destructive laboratory testing of structural members and components is both meaningful and routine. The shells community now faces the uncomfortable reckoning that existing test databases are of little quantitative value for modern design practice, except perhaps to act as a sandbox to train new researchers in methods of shell buckling, statistical analysis and experimental mechanics. The above also indicates that a meaningful calibration of safety factors, as undertaken for example by Sørensen and Toft [56], cannot produce a viable outcome based on available test results. Since obtaining test data for large scale structures is not feasible, it will remain impossible to determine partial safety factors based on testing as required by EN 1990 [59]. The partial safety factor of $\gamma_{M1} = 1.1$ in the current 2007 version of EN 1993-1-6 [54] has been retained into the latest 2022 draft prEN 1993-1-6 [58] only because historical precedence does not yet indicate that it should be changed to a higher value.

9. Conclusions

This study has demonstrated that it is conceivable that a synthetic dataset of 'tests' that shares the statistical characteristics of an actual observed dataset can be generated solely using nonlinear finite element analysis, provided that accurate inputs are available concerning the geometric ranges, local and global geometric imperfections, load application non-uniformity and material properties. This finding then establishes the possibility of using varied synthetic datasets for the accurate and meaningful calibration of design equations established under nominal variable assumptions governing the resistance of civil engineering metal shells under different load conditions. This is particularly pertinent in structural applications that push the boundaries of knowledge and the scope of validity of established design rules to meet the growing needs of society, such as the drive to construct ever taller wind turbine towers to access higher wind speeds and maximise power output.

The data necessary for the generation of such synthetic datasets, for example high-quality surface geometric imperfection surveys of the shell wall, local connections and boundaries, is now readily obtainable with modern non-destructive optical technologies. However, it is acknowledged that surface imperfection surveys alone may be insufficient for low to intermediate slenderness shells and may need to be supplemented by information regarding local residual stresses or other manufacturing defects. This is particularly the case if robust synthetic datasets are to be generated for ultimate limit states other than stability.

Declaration of Competing Interest

The authors declare that they have no known competing financial interests or personal relationships that could have appeared to influence the work reported in this paper.

Data availability

Data will be made available on request.

Appendix A. Supplementary data

The collected dataset may be downloaded in Excel format from the Authors' ResearchGate profiles as well as via the following GitHub link:

https://github.com/SadowskiAJ/MC-Paper-Dataset.git.

Supplementary data to this article can be found online at https://doi.org/10.1016/j.strusafe.2022.102285.

References

[1] Lorenz R. Achsensymmetrische Verzerrungen in dünnwandigen Hohlzylindern. Zeitschrift des Vereines Deutscher Ingenieure 1908;52(43):1706–13.
[2] Timoshenko SP. Einige Stabilitätsprobleme aus der Elastizitätstheorie. Zeitschrift für Mathematik und Physik 1910;58(4):337–85.
[3] Koiter WT. On the Stability of Elastic Equilibrium", (in Dutch) *PhD Thesis*, Delft University, (see also Translation AFFDL-TR-70-25 Wright Patterson Air Force Base, 1970); 1945.
[4] Singer J, Arbocz J, Weller T. Buckling experiments: experimental methods in buckling of thin-walled structures – Shells, Built-up Structures, Composites and Additional Topics –, Volume 2. New York: John Wiley & Sons Inc.; 2002.
[5] Elishakoff I, Li W, Starnes Jr JH. Non-classical problems in the theory of elastic stability. Cambridge University Press; 2001.

[6] Elishakoff I. Uncertain buckling: its past, present and future. Int J Solids Struct 2000;37:6869–89.
[7] Elishakoff I. Probabilistic resolution of the twentieth century conundrum in elastic stability. Thin-Walled Struct 2012;59:35–57.
[8] Elishakoff I. Resolution of the twentieth century conundrum in elastic stability. World Scientific Publishing Co.; 2014.
[9] von Kármán T, Tsien H-S. The buckling of thin cylindrical shells under axial compression. J Aeronautical Sci 1941;8:302–12.
[10] Kempner J. Postbuckling behaviour of axially compressed circular cylindrical shells. J Aeronautical Sci 1954;21:329–35.
[11] Koiter WT. A consistent first approximation in the general theory of thin elastic shells, in W.T. Koiter (Ed.) *Proc. Symp. on the Theory of Thin Elastic Shells*, North Holland; 1960, 12–33.
[12] Hoff NJ, Madsen WA, Mayers J. Postbuckling equilibrium of axially compressed circular cylindrical shells. AIAA J 1966;4:126–33.
[13] Yamaki N. Elastic stability of circular cylindrical shells. Elsevier Science; 1984.
[14] Arbocz J, Babcock Jr CD. Experimental investigation of the effect of general imperfections on the buckling of cylindrical shells. *NASA Report CR-1163*; 1968.
[15] Arbocz J, Babcock Jr CD. The effect of general imperfections on the buckling of cylindrical shells. ASME J Appl Mech 1969;36:28–38.
[16] Jullien J-F, Limam A, Gusic G. Cylindrical shells buckling under external pressure: influence of localised thickness variation. *Proc., International Conference on Advances in Steel Structures*, ICASS'99, Vol. 2, Hong Kong, December 1999, pp. 613-620; 1999.
[17] Bushnell D. Computerised buckling analysis of shells. Dordrecht: Martinus Nijhoff Publishers; 1985.
[18] Teng JG, Rotter JM. In: Buckling of thin shells: An overview Chapter 1 in *Buckling of Thin Metal*. Spon Press; 2004. p. 1–41.
[19] Harris LA, Suer HS, Skene WT, Benjamin RJ. The stability of thin-walled unstiffened circular cylinders under axial compression include the effects of internal pressure. J Aeronautical Sci 1957;24(8):587–96.
[20] Weingarten VI, Morgan EJ, Seide P. Elastic stability of thin-walled cylindrical and conical shells under axial compression. AIAA J 1965;3(3):500–5.
[21] Schulz U. Der Stabilitätsnachweis bei Schalen. *Berichte der Versuchsanstalt für Stahl, Holz und Steine*, 4(2), University of Karlsruhe; 1981.
[22] Ummenhofer T. Stabilitätsverhalten imperfekter zylindrischer Stahlsiloschalen – experimentelle und numerische Untersuchungen. *Berichte der Versuchsanstalt für Stahl, Holz und Steine*, 5(2), University of Karlsruhe; 1997.
[23] Waeteraere KP. Überprüfung der experimentellen Absicherung der Beulkurve für sehr imperfektionsempfindliche Schalenbeulfälle in der zukünftigen DIN 18800–4 am Beispiel der axialgedrückten Kreiszylinderschale. Germany: University of Duisburg-Essen; 1988. Diploma Dissertation.
[24] Schmidt H. Dickwandige Kreiszylinderschalen aus Stahl unter Axialdruckbelastung. Stahlbau 1989;58(5):143–8.
[25] Wagner HNR, Hühne C, Elishakoff I. Probabilistic and deterministic lower-bound design benchmarks for cylindrical shells under axial compression. Thin-Walled Str 2020;146:106451.
[26] Jiao P, Chen Z, Tang X, Su W, Wu J. Design of axially loaded isotropic cylindrical shells using multiple perturbation load approach – Simulation & validation. Thin-Wld Str 2018;133:1–16.
[27] Wang B, Zhu S, Hao P, Bi X, Du K, Chen B, et al. Buckling of quasi-perfect cylindrical shells under axial compression: A combined experimental and numerical investigation. Int J Solids Struct 2018;130–131:232–47.
[28] Wang B, Du K, Hao P, Tian K, Chao YJ, Jiang L, et al. Experimental validation of cylindrical shells under axial compression for improved knockdown factors. Int J Solids Struct 2019;164:37–51.
[29] NASA SP-8007 (1965, rev. Buckling of thin-walled circular cylinders 1968 NASA Space Vehicle Design Criteria National Aeronautics and Space Administration, Springfield VA, USA.
[30] Koiter WT. The effect of axisymmetric imperfections on the buckling of cylindrical shells under axial compression. Koninklike Nederlandische Akad. van Wetenshappen Proc Ser 1963;B66:265–79.
[31] Hutchinson JW. Axial buckling of pressurised imperfect cylindrical shells. AIAA J 1965;3:1461–6.
[32] Tennyson RC, Muggeridge DB. Buckling of axisymmetric imperfect circular cylindrical shells under axial compression. AIAA J 1969;7(11):2127–31.
[33] de Vries J, The Imperfection Data Bank and its Applications. PhD Thesis 2009 TU Delft.
[34] Antoine PO. Comportement des coques cylindriques minces sous chargements combinés: vers une amélioration du dimensionnement sous flexion et pression interne (Behaviour of thin cylindrical shells under combined loading: towards an improved design process for bending and internal pressure). France: INSA de Lyon, Lyon; 2000. PhD thesis.
[35] Ding XL, Coleman RD, Rotter JM. Technique for precise measurement of large-scale silos and tanks. ASCE J Surveying Eng 1996;122(1):14–25.
[36] Teng JG, Lin X, Rotter JM, Ding XL. Analysis of geometric imperfections in full-scale welded steel silos. Eng Struct 2005;27(6):938–50.
[37] Berry PA, Rotter JM, Bridge RQ. Compression tests on cylinders with circumferential weld depressions. ASCE J Eng Mech 2000;126(4):405–13.
[38] Hühne C, Rolfes R, Breitbach E, Teßmer J. Robust design of composite cylindrical shells under axial compression – Simulation and validation. Thin-Walled Struct 2008;46:947–62.
[39] Degenhardt R, Kling A, Bethge A, Orf J, Kärger L, Zimmerman R, et al. Investigations on imperfection sensitivity and deduction of improved knock-down factors for unstiffened CFRP cylindrical shells. Compos Struct 2010;92:1939–46.
[40] Sadowski AJ, van Es SHJ, Reinke T, Rotter JM, Gresnigt AM, Ummenhofer T. Harmonic analysis of measured initial geometric imperfections in large spiral welded carbon steel tubes. Eng Struct 2015;85:234–48.
[41] Hilburger MW, Nemeth MP, Starnes Jr JH. Shell buckling design criteria based on manufacturing imperfection signatures. AIAA J 2006;44(3):654–63.
[42] Hilburger MW. On the development of shell buckling knockdown factors for stiffened metallic launch vehicle cylinders. *Proc. AIAA/ASCE/AHS/ASC Structures, Structural Dynamics and Materials Conference*, 8-12 January, Kissimmee, Florida; 2018.
[43] Athiannan K, Palaninathan R. Experimental investigations on buckling of cylindrical shells under axial compression and transverse shear. Sadhana 2004;29 (1):93–115.
[44] Wagner HNR, Hühne C, Janssen M. Buckling of cylindrical shells under axial compression with loading imperfections: an experimental and numerical campaign on low knockdown factors. Thin-Walled Struct 2020;151:106764.
[45] Wagner HNR, Hühne C, Niemann S, Khakimova R. Robust design criterion for axially loaded cylindrical shells – Simulation and validation. Thin-Walled Struct 2017;115:154–62.
[46] Groh RMJ, Pirrera A Localized post-buckling states of axially compressed cylinders and their energy barriers. *Proc. AIAA Scitech 2019 Forum,* 7-11 Jan., San Diego, CA; 2019.
[47] Groh RMJ, Pirrera A. On the role of localizations in buckling of axially compressed cylinders. Proc R Soc A 2019;475:20190006.
[48] DIN 18800-4. Stahlbauten – Stabilitätsfälle, Schalenbeulen. *Deutsches Institut für Normung*, Berlin; 1990.
[49] Rotter JM. Buckling under axial compression, in Design of Steel Bins for the Storage of Bulk Solids, edited by J.M. Rotter, University of Sydney, March 1985, pp 122-137; 1985.
[50] Rotter JM. Buckling of cylindrical shells under axial compression. In: Teng JG, Rotter JM, editors. Buckling of Thin Metal Shells. London: Spon; 2004. p. 42–87.
[51] ENV 1993-1-6. Eurocode 3: Design of steel structures, Part 1. 6: General rules - Supplementary rules for the strength and stability of shell structures. Brussels: Comité Européen de Normalisation; 1999.
[52] Rotter JM. Proposal for cylinder axial compression buckling strength to be described in terms of amplitude of imperfection. Report to standards drafting panels ECCS TWG8.4 Buckling of Shells, CEN TC250/SC3 PT3 (Chimneys and Towers) and PT4 (Silos, Tanks and Pipelines), May; 1995.
[53] Rotter JM. Development of proposed European design rules for buckling of axially compressed cylinders. Adv Struct Eng 1998;1(4):273–86.
[54] EN 1993-1-6. Eurocode 3: Design of Steel Structures. Part 1–6: Strength and Stability of Shell Structures. Brussels: Comité Européen de Normalisation; 2007.
[55] Schmidt H, Rotter JM, Greiner R. Rules for the buckling limit state assessment using stress design" in Stability of Steel Shells: European Design Recommendations: 5th Edn, Eds J.M. Rotter and H. Schmidt, European Conv. for Constr. Steelwork, Brussels; 2008 & 2013, pp 147–165.
[56] Sørensen JD, Toft HS. Safety factors – background document. *DTU Wind Energy E-Report-0066*. Technical University of Denmark; 2014.
[57] IEC 61400-1. Wind energy generation systems – Part 1: Design requirements. Geneva: International Electrochemical Commission; 2019.
[58] prEN 1993-1-6, Eurocode 3: Design of Steel Structures. Part 1–6: Strength and Stability of Shell Structures 2021 Final Document Comité Européen de Normalisation, Brussels.
[59] En 1990, Eurocode – Basis of structural design 2002 Comité Européen de Normalisation Brussels.
[60] Rotter JM. Shell buckling and collapse analysis for structural design: the new framework of the european standard. In: Drew HR, Pellegrino S, editors. New Approaches to Structural Mechanics, Shells and Biological Structures. Publishers: Kluwer Academic; 2002. p. 355–78.
[61] En 1993-1-1, Eurocode 3: Design of Steel Structures. Part 1–1: General rules and rules for buildings 2005 Comité Européen de Normalisation Brussels.
[62] En 1993-1-4, Eurocode 3: Design of Steel Structures. Part 1–4: General rules – Supplementary rules for stainless steels 2006 Comité Européen de Normalisation Brussels.
[63] Afshan S, Francis P, Baddoo NR, Gardner L. Reliability analysis of structural stainless steel design provisions. J Constr Steel Res 2015;114:293–304.
[64] Buchanan C, Gardner L, Liew A. The continuous strength method for the design of circular hollow sections. J Constr Steel Res 2016;118:207–16.
[65] Zhao O, Gardner L, Young B. Structural performance of stainless steel circular hollow sections under combined axial load and bending – Part 1: Experiments and numerical modelling. Thin-Walled Struct 2016;101:231–9.
[66] Zhao O, Gardner L, Young B. Structural performance of stainless steel circular hollow sections under combined axial load and bending – Part 2: Parametric studies and design. Thin-Walled Struct 2016;101:240–8.
[67] Meng X, Gardner L. Cross-sectional behaviour of cold-formed high strength steel circular hollow sections. Thin-Walled Struct 2020;156:106822.
[68] Meng X, Gardner L, Sadowski AJ, Rotter JM. Elasto-plastic behaviour and design of semi-compact circular hollow sections. Thin-Walled Struct 2020;148:106486.
[69] Peterson JP, Dow MB. Compression tests on circular cylinders stiffened longitudinally by closely spaced Z-section stringers. *NASA Memo 2-12-59L*, Washington; 1959.
[70] Dongxu L, Uy B, Aslani F, Hou C. Behaviour and design of spiral-welded stainless steel tubes subjected to axial compression. J Constr Steel Res 2019;154:67–83.
[71] Makarov BP. Application of a statistical method for analysis of experimental data on shell stability. Izvestiya Akademii Nauk, SSSR, Otdelenie Tekhnicheskikh Nauk, Mekhanika i Mashinostroenie 1962;1:157–8. in Russian.

[72] Makarov BP. Application of statistical method for analysis of nonlinear problems of shell stability, *Theory of Plates and Shells, Proc. of the All-Union Conference*, Kiev, pp. 363–7, 1962b (in Russian).
[73] Makarov BP. Analysis of nonlinear shell stability problems with the aid of a statistical method. Inzhenernyi Zhurnal 1963;3:100–6. in Russian.
[74] Yamaki N, Otomo K, Matsuda K. Experiments on the postbuckling behaviour of circular cylindrical shells under compression. Exp Mech 1975;15:23–8.
[75] Schmidt H. Two decades of research on the stability of steel shell structures at the University of Essen (1985–2005): Experiments, evaluations, and impact on design standards. Adv Struct Eng 2018;21(16):1–29.
[76] Rotter JM, Al-Lawati H. Length effects in the buckling of imperfect axially compressed cylinders. Proc. SDSS 2016, International Colloquium on Stability and Ductility of Steel Structures, 30 May - 1 June, Timisoara, Romania; 2016, pp 631–638.
[77] Sadowski AJ, Rotter JM, Reinke T, Ummenhofer T. Statistical analysis of the material properties of selected structural carbon steels. Struct Saf 2015;53:26–35.
[78] Rotter JM. Design standards and calculations for imperfect pressurised axially compressed cylinders. *Proc. Int. Conf. on Carrying Capacity of Steel Shell Structures*, Brno, 1-3 October, 354-360; 1997.
[79] Fajuyitan OK, Sadowski AJ. Imperfection sensitivity in cylindrical shells under uniform bending. Adv Struct Eng 2018;21(16):2433–53.
[80] Ben Saïda A. Shapiro-Wilk and Shapiro-Francia normality tests" *Matlab Central File Exchange*, https://www.mathworks.com/matlabcentral/fileexchange/13964-shapiro-wilk-and-shapiro-francia-normality-tests, retrieved on May 24, 2021.
[81] Osgood WR. The crinkling strength and the bending strength of round aircraft tubing. *NACA Report N. 632*; 1938.
[82] Kanemitsu S, Nojima NM. Axial compression test of thin circular cylinders. Thesis: California Institute of Technology; 1939.
[83] ArcelorMittal. Steel foundation solutions – general catalogue 2021. *Commercial Brochure*, Luxembourg; 2021.
[84] Arianspace. Arianspace Launch Services Company. *Online resource*, https://www.arianespace.com/, accessed on 28/04/21; 2021.
[85] Steel Construction. Interactive 'blue book'. *Online resource*, https://www.steelforlifebluebook.co.uk/, accessed on 28/04/21; 2021.
[86] ABAQUS. ABAQUS 2020 Commercial Finite Element Software and Documentation. Dassault Systèmes: Simulia Corporation, Providence, RI, USA; 2020.
[87] Brush DO, Almroth BO. Buckling of bars, plates and shells. McGraw Hill; 1975.
[88] Calladine CR. Theory of shell structures. Cambridge University Press; 1983.
[89] Teng JG, Rotter JM. Buckling of pressurised axisymmetric imperfect cylinders under axial loads. ASCE J Eng Mech 1992;118(2):229–47.
[90] Song CY, Teng JG, Rotter JM. Imperfection sensitivity of thin elastic cylindrical shells subject to partial axial compression. Int J Solids Struct 2004;41:7155–80.
[91] Sadowski AJ, Pototschnig L, Constantinou P. The 'panel analysis' technique in the computational study of axisymmetric thin-walled shell systems. Fin Els Anal Dsgn 2018;152:55–68.
[92] Wang J, Fajuyitan OK, Orabi MA, Rotter JM, Sadowski AJ. Cylindrical shells under uniform bending in the framework of Reference Resistance Design. Jrnl Cnst. Stl Rsrch 2020:166.
[93] Riks E. An incremental approach to the solution of snapping and buckling problems. Int J Solids Struct 1979;15:529–51.
[94] Sadowski AJ, Fajuyitan OK, Wang J. A computational strategy to establish algebraic parameters for the Reference Resistance Design of metal shell structures. Adv Eng Softw 2017;109:15–30.
[95] Holst JMFG, Rotter JM. Axially compressed cylindrical shells with local settlement. Thin-Walled Struct 2005;43:811–25.
[96] Mooney CZ. Monte Carlo Simulation" *Sage University Paper Series on Quantitative Applications in the Social Sciences*, N. 07-116, Newbury Park, CA. 1997.
[97] Henkel RE. Tests of significance *Sage University Paper Series on Quantitative Applications in the Social Sciences*, N. 07-004, Newbury Park, CA; 1976.
[98] Efron B, Tibshirani RJ. An introduction to the bootstrap. Monographs on statistics and applied probability. Chapman & Hall / CRC Press; 1994.
[99] Esslinger M. Hochgeschwindigkeitsaufnahmen vom Beulvorgang dünnwandiger axialbelasteter Zylinder. Der Stahlbau 1970;39:73–6.
[100] Wagner HNR, Hühne C, Zhang J, Tang W, Khakimova R. Geometric imperfection and lower-bound analysis of spherical shells under external pressure. Thin-Walled Struct 2019;143:106195.